© smp chair committee (Kourosh Koushan and Sverre Steen)
DOI: 10.15480/882.9365

Eighth International Symposium on Marine Propulsors
smp'24, Berlin, Germany, March 2024

An Investigation into the Effect on Ship Manoeuvring of a Pre-Swirl Duct

Steven Leonard[1], Lars Lübke[2]

[1]IBMV Maritime Innovationsgesellschaft mbH (ibmv), Rostock, Germany
[2]Ship Model Basin Potsdam (SVA), Potsdam, Germany

ABSTRACT

To date, pre-swirl ducts (PSDs) have been developed primarily from the viewpoint of improving propulsion efficiency. Such devices tend to add a substantial wetted surface area at the aft end of a vessel, but little is known on how this affects a vessel's overall manoeuvring qualities. Becker Marine Systems (BMS), ibmv, SVA Potsdam and the Technische Universität Hamburg-Harburg (TUHH) have therefore initiated a joint research project to further investigate the influence of PSDs on the manoeuvring abilities of ships. The work has been focused on two key aspects. Firstly, the complex interaction between ship, PSD, propeller and rudder was studied via numerical simulations correlated against extensive wind tests for various configurations of propeller, rudder and PSD and different drift angles. Secondly, manoeuvring investigations were carried out to determine the influence of PSDs on the key manoeuvring parameters. This included testing in both the towing tank and free-running tests on a lake, with comparisons made against equivalent CFD simulations. To enable reasonable computation time the manoeuvring CFD simulations used a body-force propeller model. The measurement campaign encompassed turning circles, zig-zag tests (10°/10° and 20°/20°) as well as spiral manoeuvres, with and without various PSDs fitted. For this work the JBC model was selected.

The investigations show that the PSD only marginally influences the manoeuvring behaviour of full-form ships. The JBC hull is slightly unstable with respect to yaw. The yaw instability is primarily related to flow separation in the aft part of the ship above the propeller. In this case, PSDs are not able to impose significant changes to the unstable region.

Keywords

Energy-saving devices (ESD), Pre-swirl ducts (PSD), Manoeuvring, CFD, yaw instability.

1 INTRODUCTION

With the advent of EEDI and EEXI rules for ship efficiency, recent years have seen the fitting of PSDs become established in both the new-build and retrofit markets. The Becker Mewis Duct ™ was introduced to the market in 2008. It is positioned directly in front of the propeller and combines a series of fins concentric to a fully- or partly-surrounding duct ring. In Figure 1, a typical Becker Mewis Duct installation is shown. To date, over 1600 of these devices are fitted to ships worldwide.

Figure 1: Typical installation of a Becker Mewis Duct ™

Becker Mewis Ducts are optimised purely with the goal of minimising delivered power in the straight ahead, calm-water condition, as demonstrated exemplarily by Guiard et al (2013). CFD techniques are used extensively for this process, with final adjustment and proof-of-performance usually obtained via model basin self-propulsion testing. As such, almost no attention has been paid to the impact of PSDs on the vessel's maneuvering behavior and consequently little is yet known about these aspects. In particular, any changes to vessel yaw stability are of prime interest.

There exists some anecdotal feedback from operators where a PSD has been retrofitted to certain vessels regarding reduced vibrations on the bridge or, with respect to maneuvering, that the directional stability is improved. However, the information is of little value when the possible degree of change cannot be quantified.

Published data on the effect of PSDs on ship manoeuvring are scarce. Kishimoto et al (2016) detail a series of model-basin free-running manoeuvring tests using the JBC bulk carrier hull fitted with and without the JBC duct. The manoeuvres studied include turning circle, 10°/10° zig-zag and oblique tests, and showed no appreciable adverse effects on the manoeuvring performance.

A joint research project (PSDMan: Pre-Swirl Duct Manoeuvring) was therefore initiated with the aim of

increasing the understanding of how a PSD affects a ship's manoeuvring qualities. The project consisted of four partners, namely the Schiffbau-Versuchsanstalt (SVA) Potsdam, ibmv, the Institute of Fluid Dynamics & Ship Theory at the Technical University of Hamburg (TUHH) and Becker Marine Systems (BMS), who acted as project coordinator. Each partner contributed to the project according to their facilities and expertise.

Within the TUHH comprehensive wind tunnel tests were carried out, employing a tomographic "3D3C" PIV system to measure detailed flow properties around the duct. SVA Potsdam would perform initial towing tank tests to prove the powering performance, and also undertake a series of manoeuvring tests on an external lake. For ibmv the task was primarily CFD-focused, using the measured results from TUHH and SVA Potsdam for validation. Particular emphasis was placed on developing a CFD procedure to quickly and reliably model the manoeuvring qualities of a vessel with and without a PSD fitted. In addition to this, ibmv was also responsible for the PSD designs. All investigations were conducted for a variety of hull, PSD, rudder and propeller configurations.

2 GEOMETRY

For these investigations the well-known JBC (Japan Bulk Carrier) model was chosen, since the geometry is freely available and used in various CFD workshops (Hino et.al.2021) providing a broad base of publications and validation data. In Table 1 the main particulars of the hull and the original propeller are given for full-scale. The geometry of the hull is shown in Figure 2.

Table 1: Main particulars of ship

JBC (full-scale)			
Length b. perpendiculars	L_{PP}	[m]	280.00
Breadth	B	[m]	45.00
Draught	T	[m]	16.50
Displacement	∇	[m³]	178370
Original propeller (P687)			
Diameter	D	[m]	8.12
Pitch	$P_{0.7}/D$	[–]	0.75
Area ratio	A_E/A_0	[–]	0.50
Number of blades	Z	[-]	5

For wind-tunnel measurements a 1/80 scale double-hull model was used, whereas for model basin and manoeuvring tests at SVA a larger 1/40 scale was adopted. The design draught, corresponding to 16.5m in full-scale, was used throughout.

The rudder for the JBC is a traditional semi-spade design, and therefore difficult to model with CFD during transient motions of the rudder blade. Since rudder performance was not of core interest it was re-designed as a full-spade rudder with fixed skeg, using the NACA-0063 profile as a basis. This revised rudder was used for all CFD simulations and model testing. The spade rudder has a span of 11.5 m and mean chord of 7.05 m, these dimensions being based on BMS standard sizing for the given ship particulars. The resulting geometry can also be seen in Figure 2.

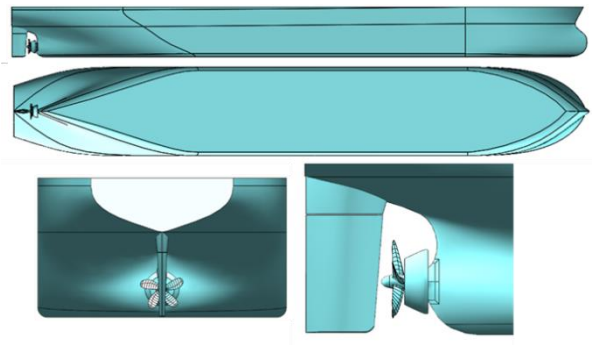

Figure 2: JBC hull, with spade rudder and duct

The JBC is provided with a duct of wake equalizing type, consisting of a single vertical fin surrounded by a full duct ring set at a large pitch angle, see Figure 2. This original duct is denoted D0. Two additional Mewis Duct designs were developed for this project. The first duct, D1, was designed and optimized for delivered power, using the standard ibmv procedure for slow, full-form vessels and assuming that the JBC propeller was fitted and without any consideration of manoeuvring properties.

A second duct, D2, was subsequently developed to suit a modified propeller designed by SVA Potsdam, and incorporate potential performance improvements identified during the first duct design process. The results of the second propeller are not presented here, since they do not provide additional insight to the present topic. This duct is of larger overall diameter, with an identical fin layout, but the fins adapted in pitch along their span to suit the local wake direction. The main particulars of the ducts are given in Table 3. The PSDs D1 and D2 are shown in more detail in Figure 3.

Table 2: Main particulars of ducts

Ducts			**D0**	**D1**	**D2**
Diameter	D	[m]	4.46	5.20	5.60
Chord length	c	[m]	2.44	2.00	2.36

Figure 3: Pre-swirl ducts viewed from ahead

For the towing tank and free manoeuvring tests, a wooden model was manufactured, with the propellers milled from brass. For the wind tunnels tests both the ship model and

propeller were made from fibre-reinforced plastic and painted with a Rhodamin layer to reduce laser reflections. The PSDs were manufactured via 3D-printing.

3 MEASUREMENTS

Different measuring campaigns in the different facilities were carried out, which encompassed resistance and propulsion tests in the towing tank of the SVA Potsdam, manoeuvring tests with a free-running model on a lake and wind tunnels test in the TUHH.

For the propulsion and manoeuvring tests, the same ship model was used, but instrumented differently. For the manoeuvring tests the model was fitted such that it could be remotely operated, or that pre-defined manoeuvres could be programmed and executed. The communication with the land-based control station was accomplished with radio signals. A battery pack guaranteed the power supply for the electric motor and the measuring equipment. To track the position and the velocity a GPS-system was installed, with rotational movements and accelerations measured via a gyroscope. The free-running tests were carried out with a constant rate of revolution according to the propulsion prognosis. The delivered power was restricted in accordance with an assumed motor limit. In Figure 4 the JBC model as operated during the manoeuvres is shown.

Figure 4: Free-running manoeuvring tests

To study the interaction of the different components of the propulsion system with the PSD, and to assess the maximum loads on the PSD models during manoeuvring, the duct forces were measured throughout. The sensor was integrated into the hull, positioned below the shaft axis. The duct, fins and brackets were manufactured from a single piece and mounted directly on the sensor, having a cylindrical opening for the propeller shaft. The external fairing, in form of the ship contour, covers the sensor and the fins without contact. The design incorporates a minimum clearance of about 1 mm. In Figure 5 the measuring system is shown, with the sensor in grey, the duct in green and the fairing in purple, blue and red. Besides the duct, rudder and propeller forces, the position and the kinematic data of the model was monitored.

The wind tunnel tests were conducted in the wind tunnel facility of the TUHH, having a test section with a rectangular cross section of 2 m × 3 m and a length of 5.5 m. The wind tunnel can be operated in a closed (Göttingen) or open (Eiffel) mode, with maximum wind speeds of 35 m/s. Stereo and Tomographic Particle Image Velocimetry (S-PIV and T-PIV) were used to measure the flow field. The PIV systems are operated with lasers of Nd:YAG and Nd:YLF type, with two or four 4MP-cameras of different resolutions. The T-PIV system can be operated with a maximum sampling rate of 1.1 kHz.

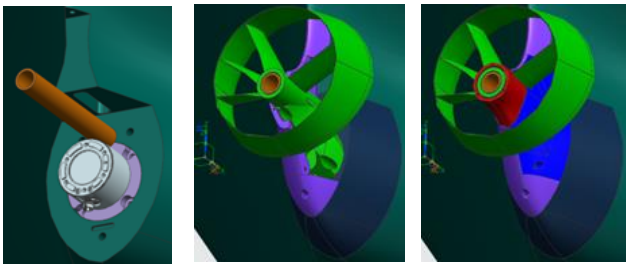

Figure 5: Sensor for measurement of duct forces

In Figure 6 the cable-suspended double-body model of the JBC in the wind tunnel is shown.

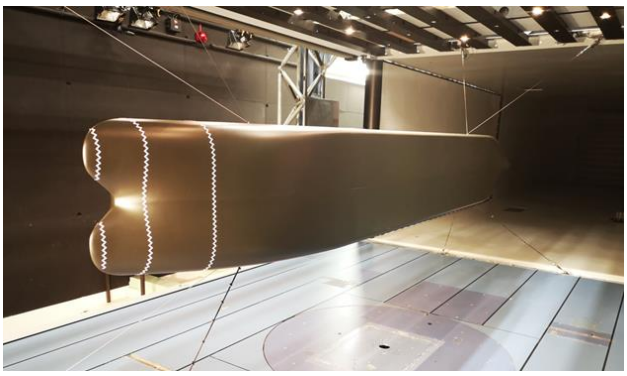

Figure 6: Wind tunnel tests

4 PROPULSION TESTS

Propulsion tests were carried out to check the resulting powering performance of the three PSDs D0, D1 and D2.

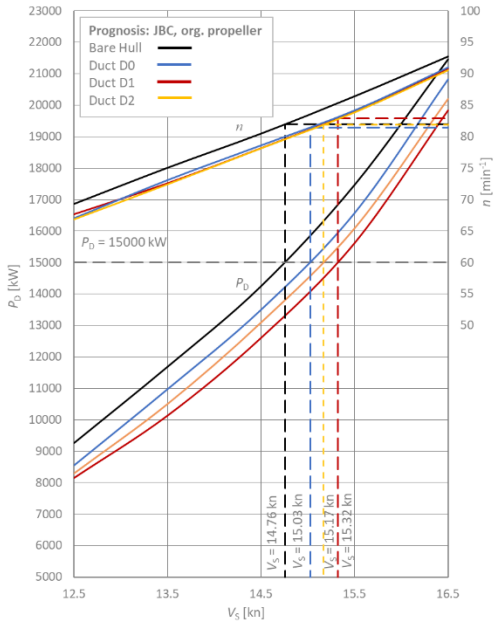

Figure 7: Speed prognosis for JBC with different ducts

For the propulsion prognosis for the full-scale ship, the available power was taken to be P_D = 15 MW. Measurements showed that with the duct D1 the greatest

power gains were achieved. For the propulsion efficiency the increase in duct diameter of D2 was not beneficial.

The rates of revolution for the manoeuvring tests were derived under consideration of 25 % sea margin on basis of the propulsion tests.

5 CFD COMPARISON WITH WIND TUNNEL MEASUREMENTS

Comprehensive PIV measurements at a series of transverse planes towards the aft end of the model for various configurations of rudder, propeller and duct were conducted at drift angles of 0° and 8° and a wind tunnel speed of 10 m/s. The wind tunnel measurement program formed an extension to earlier JBC hull measurements carried out with previous-generation PIV equipment, which were summarised in Shevchuck et al (2020). In Figure 8 the transverse planes for the laser flow-field measuring campaign are shown.

The aim of the investigations was to validate the computational results of the complex flow field in the aft ship against the measurements for design and off-design conditions. This step was considered important to ensure that the interaction between the different components was sufficiently well-captured with the chosen numerical setup, and that the mesh details were adequate to resolve the flow field, before proceeding towards full manoeuvring simulations. More detailed measurement results and comparisons with CFD simulations may be found in Sahab et al (2022) and Sumislawski et al (2022).

The resulting mesh cell count ranged from 20.3 million for the "hull only" case to 35.9 million for the hull with PSD and propeller. The trimmed mesher in STAR-CCM+ was used to generate the numerical mesh, with a prismatic boundary layer fulfilling $y^+ \leq 1$. The CFD simulations were undertaken with the domain boundaries positioned according to the wind tunnel section dimensions. Vertical symmetry was observed by placing a symmetry plane at the design draught.

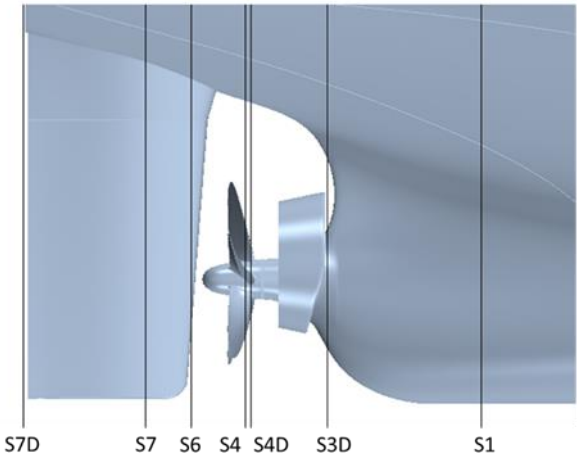

Figure 8 Location of transverse PIV measuring planes

In the following, selected results from the investigations are given. Figure 9 shows the axial velocity component at planes S1 (ahead of duct), S4D (between duct and propeller) and S7 (approximately at aft perpendicular) for the "bare hull" case at 8° drift angle, i.e. without rudder, duct or propeller fitted. For each plane the measured wind-tunnel data is on the left-hand side and the two right-most images showing the computed results using both the k-ω SST and Reynolds Stress Transport turbulence models. For both sets of CFD results the iso-countours from the wind tunnel measurements are superimposed to enable easier comparison. The equivalent results for turbulent kinetic energy are shown in Figure 10.

In terms of axial velocity, both turbulence models show good agreement of the strength, position and development of the large vortex shed from the base of the stern bulb, together with the location of the sharp velocity peak which points to starboard, located immediately above this vortex. At plane S4D, the asymmetric shape of low-velocity region near the shaft is well-captured by both models, however the RST model appears to show slightly better agreement in terms of magnitude.

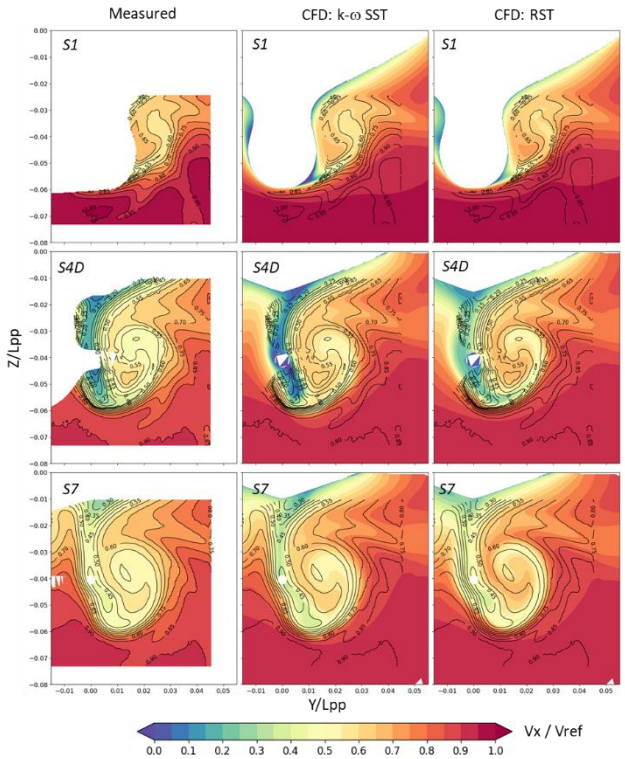

Figure 9 Comparison of measured and computed axial velocity component at different transverse planes, bare hull, 8° drift angle

The distribution of turbulent kinetic energy shows less correlation. Overall, it is clear that the CFD solutions show a significantly lower background level of kinetic energy, denoted by the darker blue colour. One possibility for this discrepancy is that the turbulence level in the tunnel is high due to the continuous recirculation of the air. Another is that the turbulence decay over the run-up to the ship model in the numerical simulation is too high, which is a common limitation of turbulence modelling. At all planes the shape of the kinetic energy field is generally well-captured by both CFD turbulence models, however the overall magnitude is consistently weaker than that measured.

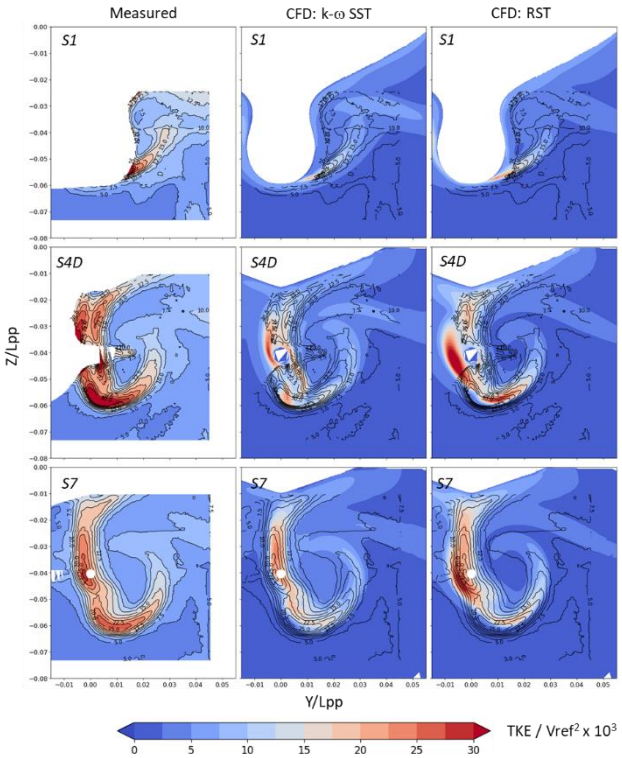

Figure 10 Comparison of measured and computed turbulent kinetic energy at different transverse planes, bare hull, 8° drift angle

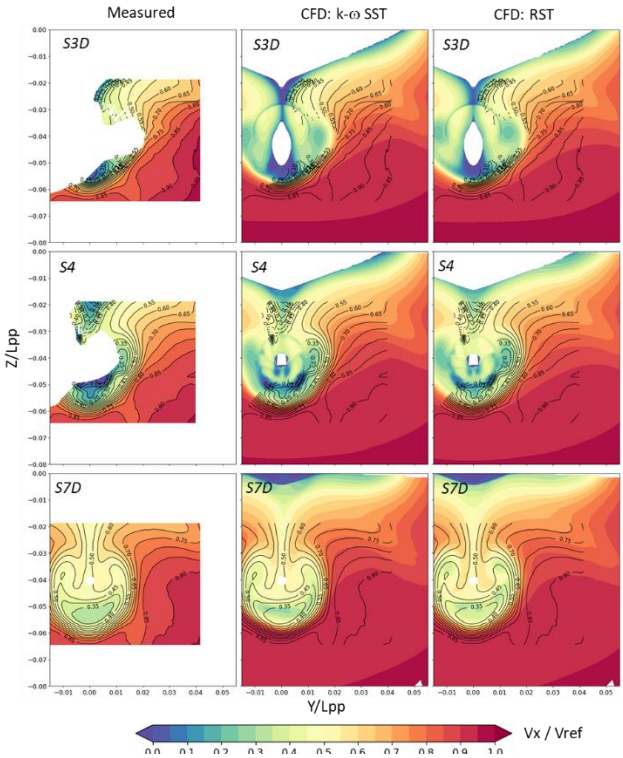

Figure 11 Comparison of measured and computed axial velocity component at different transverse planes, hull with duct D1, 0° drift angle

Figure 11 shows a comparison of the axial velocity for the hull with the duct D1 at 0° drift at different planes. The PIV measurements at S3D and S4 were not fully spatially resolved, however there is enough measured data available to suggest that both CFD turbulence models are giving good agreement in terms of both velocity magnitude and location of key flow features.

The obtained results were interpreted as encouraging for the simulation of ship manoeuvres with common two equation turbulence modelling, in this case *k-ω* SST.

6 MANOEUVRING

A key goal of the project was to obtain a sufficiently accurate and reliable CFD setup for manoeuvring simulations. It was decided to simulate the manoeuvres directly (ITTC 2021), and not to use an approach based on hydrodynamic coefficient (Abkowitz 1964), although many successful applications are published (Cura-Hochbaum 2014).

For the manoeuvring simulations the computational domain was set to an overall length of $7\times L_{PP}$, a width of $2.5\times L_{PP}$ and a depth of L_{PP}, with the vessel aft perpendicular placed at three ship-lengths aft of the upstream inlet. The domain was configured to move and rotate in the horizontal plane with the vessel. For this work the same restrictions were applied to the vessel, constraining all other degrees of freedom.

To model rudder rotation the overset mesh technique was used, with the rudder angle controlled via individual STAR-CCM+ Java macros. These macros were selected according to the manoeuvre being simulated.

The generated trimmed mesh with prismatic boundary layer was similar to that used for the comparisons with the wind tunnel measurements. The boundary layer was resolved over the entire hull, resulting in an overall cell count of about 22 million. The segregated transient solver was used with a fixed time-step of 0.05 s, which corresponds to a distance of approximately $L_{PP}/120$ per time-step at the initial ship speed of 14.5 knots. The *k-ω* SST turbulence model was selected for stability reasons, and the shaft speed set to a fixed value of 9.81 rps, which is the same as in the model tests.

In the following the simulation results of the different manoeuvres are described and briefly discussed.

6.1 Turning Circle Manoeuvre

Turning circle manoeuvres to port and starboard side with 35° rudder angle were simulated for bare hull and with the two pre-swirl ducts D1 and D2. A comparison of the vessel trajectories for the 35° starboard turning circle manoeuvre and the corresponding yaw rates for the different configurations is shown in Figure 12. The model test data is shown in blue.

The experimental and computational results are generally in a good agreement, although runaway values exist. The elliptic nature of the model test trajectories is due to environmental effects encountered during the testing. The comparison of advance and tactical diameters given in Table 3, shows that the presence of the duct has no significant effect on these parameters. The differences between measured and calculated advance turning diameters are around 9 % and for the tactical diameter between 15 %–18 %. The experimental and the

computational results show that the advance and tactical diameters are unaffected by the presence of a duct.

Table 3: Turning circle diameters, starboard 35°

JBC		b. hull	D1	D2	IMO
$D_{Advance}/L_{PP}$	EFD	2.92	2.80	3.00	4.50
	CFD	2.63	2.68	2.68	
$D_{Tactical}/L_{PP}$	EFD	2.78	2.84	2.75	5.00
	CFD	2.28	2.32	2.35	

In terms of the yaw rates, no significant effects between the hull with and without PSD can be found. In the simulations the peak yaw rate during the initial transient is marginally under-predicted, but the yaw rate decay following the initial peak is well-captured.

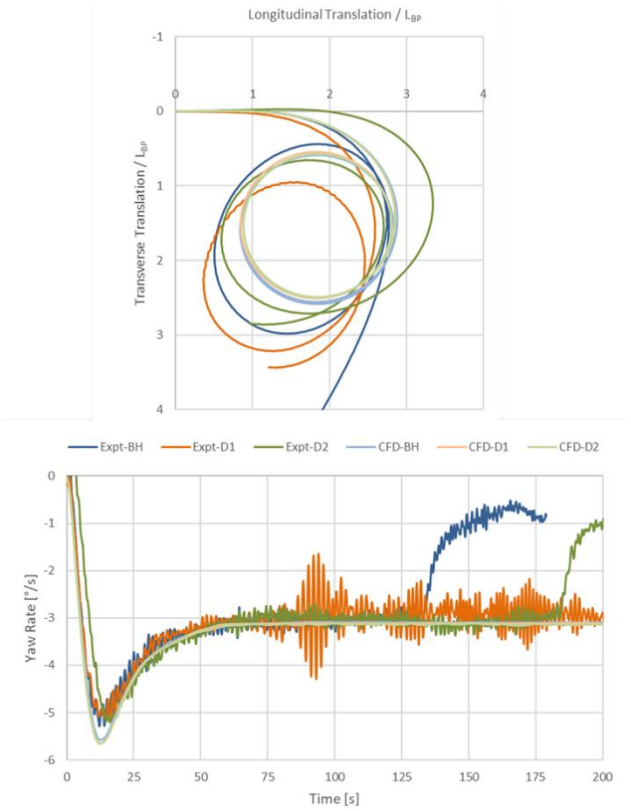

Figure 12 Trajectories (top) and yaw rate (bottom) for 35° starboard turning circle manoeuvre with different ducts

Time histories of the vessel drift angle are shown in Figure 13. Note that during model testing for the bare hull case the rudder angle was returned to zero degrees immediately following the first full circle trajectory at approximately 130 s, so the measure drift angle data for the bare hull case beyond this time can be ignored. The CFD results show that the presence of the duct tends to slightly increase both the transient and steady drift angles by a few degrees, with the steady turning phase drift angle settling at about 22° to 23°. For all three sets of measured data the drift angle does not stabilise, possibly further indicating strong environmental effects. It would appear that the mean drift angle for the D1 and D2 cases does not change significantly, and that the drift angle tends to increase when a duct is present, but it is difficult to quantify given the unsteady nature of the measurements. Overall, the CFD simulations tend to over-predict the measurements in the order of 8° to 10°. The reason for this is most likely that the free-surface was neglected in the simulations, which would otherwise restrict the drift angle.

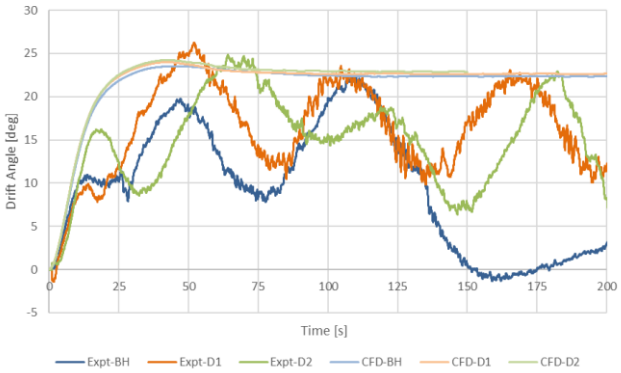

Figure 13 Time history of drift angle, 35° starboard turning circle with different ducts

Figure 14 shows a comparison of the time history of the measured and computed duct thrust and side force coefficients during the manoeuvre. The thrust coefficient values show a large discrepancy between measured and computed data for both duct designs, although both the measurements and CFD analysis suggest a large increase in thrust for the larger duct D2. Both the thrust and side force magnitudes are small, and at the limit of applicability of the force transducers, so an increased degree of measurement uncertainty is to be expected. The CFD and EFD results show an initial transient up to about 50s, from which point the mean thrust coefficient remains reasonably constant, as would be expected, since turning circles are, in essence, steady-state manoeuvres.

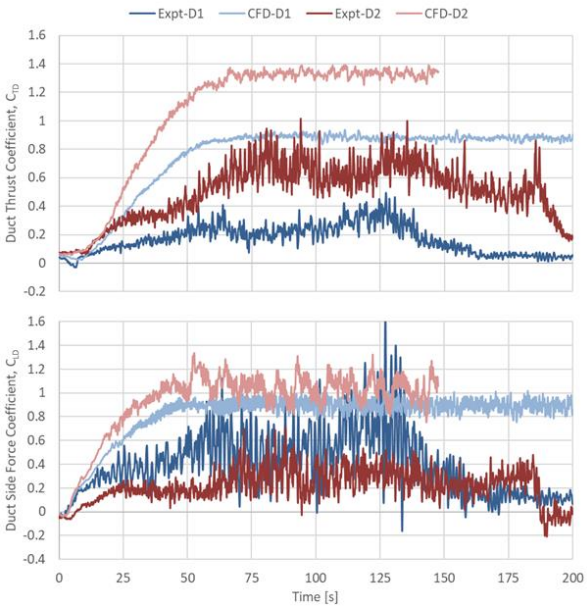

Figure 14 Time history of duct force coefficients, starboard turning circle

However, the measurements show a higher degree of unsteadiness, which may be due to environmental effects. In terms of side force coefficient, the overall correlation between EFD and CFD is again poor, in particular for D2. In addition, the CFD simulations fail to reproduce the measured high frequency unsteady force amplitudes. These unsteady force values suggest intermittent flow separation and reattachment on the PSDs.

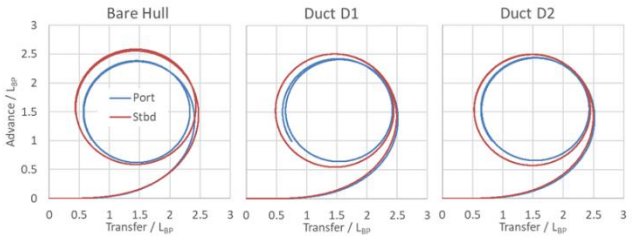

Figure 15 Difference between port and starboard turning manoeuvre

The difference between the port and starboard turning properties was evaluated for the CFD simulations only, with the corresponding trajectories given in Figure 15. Port turning is shown in blue, starboard in red. The largest effect on manoeuvring occurs with the vessel turning to starboard.

6.2 Zig-Zag Manoeuvre 10°/10°

A port-turning 10°/10° zig-zag manoeuvre is compared for the same three configurations, i.e. without PSD fitted and with ducts D1 and D2.

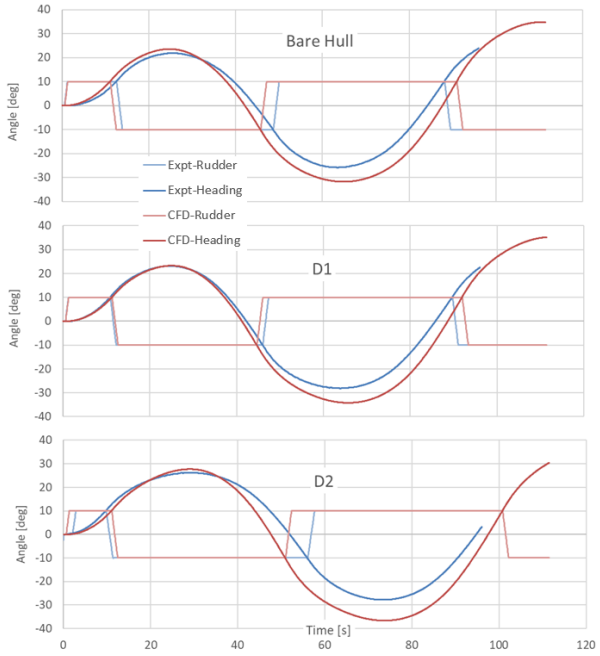

Figure 16 Comparison of overshoot angles for 10°/10° zig-zag manoeuvre

A comparison of the resulting overshoot angles is given in Figure 16. For each configuration the CFD simulations tend to over-predict the overshoot angles, the error increasing as the manoeuvre progresses. This might be due to the missing deformed free-surface in the CFD simulations. Both CFD and EFD results show that the presence of the duct increases the overshoot angle, and this increases as the duct size increases, albeit by a small value.

In Figure 17 the time history of the decay in ship velocity is shown, non-dimensionalised by the initial ship velocity. The overall trend seems to be well-predicted for all three configurations.

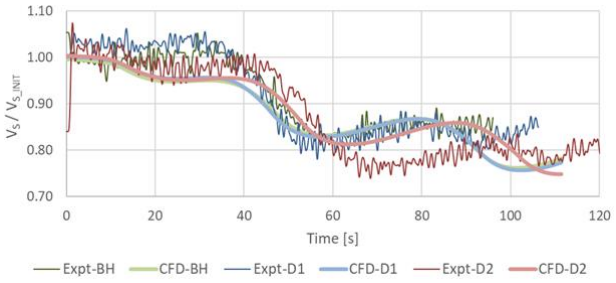

Figure 17 Comparison of ship velocity during 10°/10° zig-zag manoeuvre

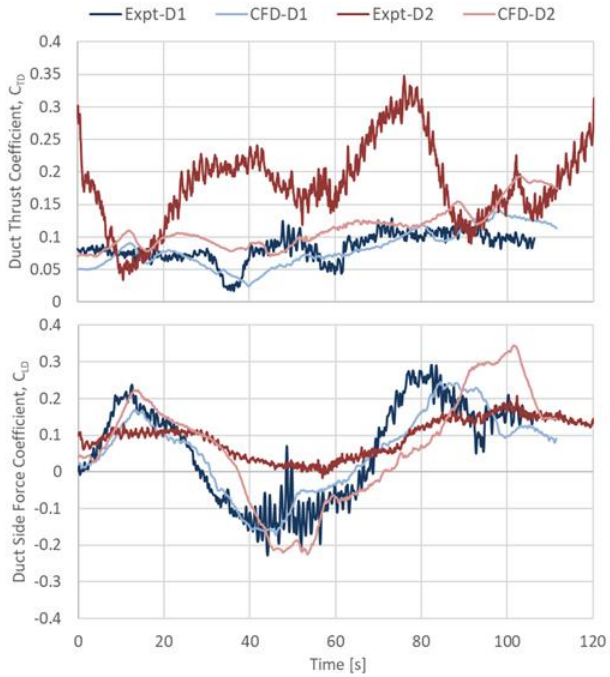

Figure 18 Comparison of duct longitudinal (thrust) and side force coefficients during 10°/10° zig-zag manoeuvre

The variation of duct longitudinal (thrust) and side force coefficients during the manoeuvre is shown in Figure 18. For duct D1 the agreement is good for both thrust and side force coefficients, although the measured higher-frequency oscillations are not captured by the RANS turbulence model, as was the case for the circle manoeuvre. For the larger duct the correlation is significantly worse. The measurements show a very large swing in peak thrust coefficient values, between 0.2 and 1.4. These values are significantly larger than those observed for D1. In contrast, the CFD simulations show slightly higher thrust coefficient values compared to D1 throughout, with almost identical trends in peak thrust positions. Conversely, the measured side force coefficient values indicate significantly smaller peak-to-peak swings for D2 relative to D1, which is in disagreement with the CFD predictions. It is noted that

both simulations and measurements show a net thrust produced by both duct designs throughout the manoeuvre. In summary, a zig-zag manoeuvre is inherently more hydrodynamically complex than a circle manoeuvre and the actuator disc model probably reveals its limited capabilities. However, the general characteristics of the flow and the interaction between the different parts is well-captured, giving rise to the conclusion that the chosen numerical setup is well-suited for low Froude-number flow.

6.3 Spiral Manoeuvre

Spiral manoeuvres were used to investigate yaw stability. One particular difficulty encountered in the simulations was accurate control and scheduling of the rudder angle. The approach adopted here was to initially prescribe the desired rudder angle steps and then continuously monitor the variance of the resulting vessel yaw rotation rate, only proceeding to the next rudder angle once the variance dropped below 0.02 °/s. The rudder rotation rate was set to the value measured during model testing and the shaft speed kept constant throughout the manoeuvre.

A comparison of the resulting steady turning rates for the three configurations is shown in the following figures. Positive rudder angles are defined for the ship turning to port, while negative for the ship turning to starboard. In Figure 19 the spiral manoeuvre starts with positive rudder angles turning the vessel to port and proceeding to negative angles and thus reversing the turning direction. In Figure 20 the manoeuvre is carried out in the opposite sense, coming from starboard and going to port side turning. The arrows indicate the direction of turning, for example, proceeding from positive to negative rudder angles as in Figure 19 or vice-versa as in Figure 20. The rudder angle increment or decrement varies between 2° and 5°.

All of the CFD predictions show a good agreement with the measurements, with the exception of the bare hull case at -5°. The measured data here is probably an outlier.

For all three configurations a hysteresis loop is evident, meaning that the ship has a different yaw rate when transitioning from positive or negative rudder angles, indicating a yaw instability. The unstable region covers roughly a rudder angle range of ±2°. The different duct configurations tend not to influence the extent of the hysteresis region, but instead the starting and ending points of the hysteresis. The differences between the ducts are rather marginal overall.

The reason for the observed yaw instability can be found in a region of flow separation above the propeller. In Figure 21 a snapshot of the swirling flow in the aft ship is shown, indicating the region where the flow separates.

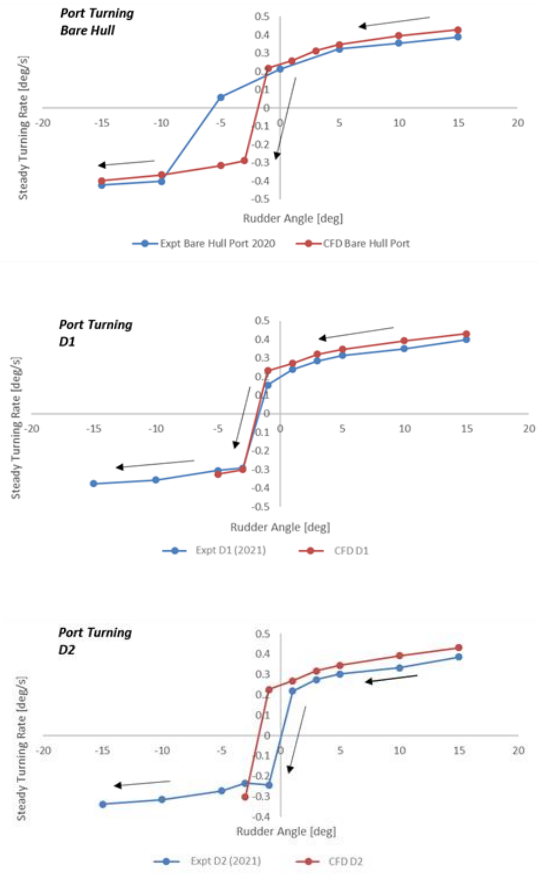

Figure 19 Comparison of spiral manoeuvre steady turning rates, starting with port side turning

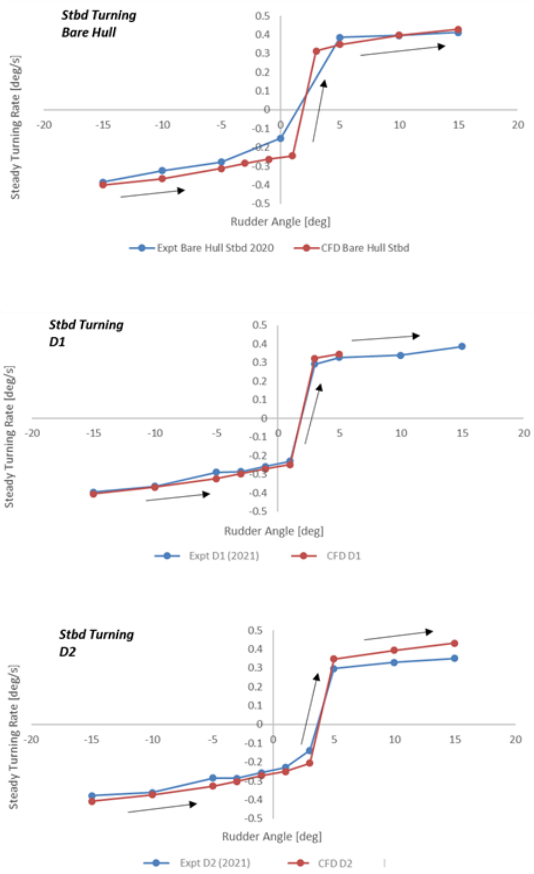

Figure 20 Comparison of spiral manoeuvre steady turning rates, starting with starboard turning

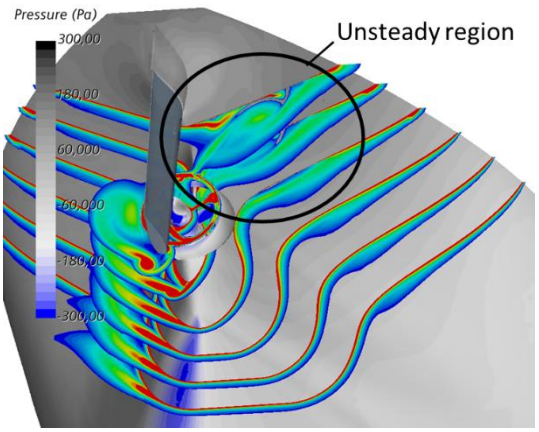

Figure 21 Computed flow separation above the propeller during the spiral manoeuvre, 2°rudder angle

7 CONCLUSIONS

To date, PSDs have been developed with the primary goal of improving the propulsion efficiency of ships. Aspects regarding their impact on the manoeuvrability have not been of major concern. This is partly due to the fact that there is no general quantitative definition for good manoeuvring properties, despite the requirement that the relevant IMO manoeuvring criteria are met. Qualitatively however, these requirements can be summarised to the extent that ships must have good course-keeping and steering characteristics, which can be contradictory.

Therefore, comprehensive numerical and experimental investigations were carried out with the JBC without and with PSDs to assess the influence of PSDs on manoeuvring behaviour. In course of the investigation's standard turning circle, zig-zag and spiral manoeuvres were considered.

A requirement for the project was to develop a robust numerical setup for these manoeuvring simulations. A key aspect of this has been to model the complex flow field at the aft ship, and thereby capture the interactions between ship, rudder, PSD and propeller sufficiently accurately. Comprehensive PIV-measurements in the wind tunnel of the TUHH were provided for validation, showing in general a good and encouraging agreement between calculations and measurements for oblique flow with and without PSDs, setting the stage for subsequent manoeuvring simulations.

In general, PSDs are fitted to ships which operate at low Froude-numbers, such as bulkers and tankers. Therefore, the deformed free-surface was neglected in the numerical setup. The propeller was modelled with a simple body-force approach. Common two-equation turbulence modelling was employed. Comparisons made with the experimental results show that the numerical calculations are in general in good agreement with the test results, leading to the conclusion that the applied restrictions are justified. The numerical setup proved to be efficient and stable.

The investigation of the turning circles showed that the PSD has only a minor impact on the tactical turning diameters. Also, PSDs with a larger lateral surface area had only marginal influence. Smaller turning circles were obtained when turning to the port side, however the PSDs have the largest influence when turning to starboard, tending to equalise the port/starboard differences.

The presence of a PSD increases the overshoot angles during zig-zag tests. Any increase in yaw stability is, however, insignificant. The evaluation of the steady yaw rates from the spiral manoeuvres shows that the JBC without duct has a slight yaw instability in the range of roughly ±2° rudder angle. The experimental and numerical results differ for a rudder angle of 5° starting with the port side turning, which might indicate that the unstable region is larger. With a PSD fitted, the unstable region is basically the same, but shifted slightly to the positive rudder angles. The reason for this instability is a region of flow separation located above the propeller, which cannot be suppressed by the presence of a PSD. Other flow instabilities may, however, be influenced by a PSD.

Further testing and simulation for faster ship types, such as container ships, and more marginally directionally stable full-form hull designs would be beneficial.

ACKNOWLEDGEMENT

The authors would like to express their gratitude to the Federal Ministry for Economic Affairs and Climate Action for funding the research project.

NOMENCLATURE

CFD		Computational fluid dynamics
EFD		Experimental fluid dynamics
ESD		Energy-saving device
PSD		Pre-swirl duct
SST		Shear Stress Transport
RST		Reynolds-Stress Transport
A_E/A_0	[-]	Expanded blade area ratio
A_R	[m²]	Rudder moveable blade area
B	[m]	Breadth of hull
c	[m]	Chord length
C_{LD}	[-]	Duct side force coefficient $F_{ZD}/(0.5\rho V_S^2 D_D^2)$
C_{LR}	[-]	Rudder side force (lift) coefficient $F_{ZR}/(0.5\rho V_S^2 A_R)$
C_{TD}	[-]	Duct thrust coefficient $F_{XD}/(0.5\rho V_S^2 D_D^2)$
D	[m]	Diameter
D_P	[m]	Propeller diameter
D_D	[m]	Duct diameter
$D_{Advance}$	[m]	Advance diameter of turning circle
$D_{Tactical}$	[m]	Tactical diameter of turning circle
F_{XD}	[N]	Duct thrust
F_{ZD}	[N]	Duct side force
F_{ZR}	[N]	Rudder side force (lift)
K_T	[-]	Propeller thrust coefficient $T_P/(\rho n^2 D_P^4)$
L_{PP}	[m]	Length between perpendiculars
n	[1/s]	Number of revolutions per second

P	[m]	Propeller pitch
P_D	[kW]	Delivered power
Re	[-]	Reynolds number $V_S L_{PP} / \nu$
T	[m]	Draught, ship
T_P	[N]	Propeller thrust
V_S	[m/s]	Velocity, ship
Z	[-]	Blade number

REFERENCES

Abkowitz, M.A., (1964), "Lectures on Ship Hydrodynamics – Steering and Manoeuvrability", HyA Report HY-5, Copenhagen

Cura-Hochbaum, A., Uharek, S. (2014), 'Prediction of the manoeuvring behaviour of the KCS based on virtual captive tests', Workshop on Verification and Validation of Ship Manoeuvring Simulation Methods

Guiard, T., Leonard, S., Mewis, F. (2013), 'The Becker Mewis duct – challenges in full-scale design and new developments for fast ships', 3rd International Symposium on Marine Propulsors

Hino, T., Stern, F., Larsson, L., Visonneau, M. (2021). Numerical Ship Hydrodynamics, An Assessment of the Tokyo 2015 Workshop. Lecture Notes in Applied and Computational Mechanics Volume 94, Springer

IMO Resolution MSC 137(76), Standards for Ship Manoeuvrability, 2002

ITTC (2021), "Guidelines on Use of RANS Tools for Manoeuvring Prediction", Recommended Procedures and Guidelines 7.5-03-04-01, 2021

Kishimoto, T., Ikeda, T., Sawata, T and Matsumura, N. (2016) 'Maneuvering Characteristics of a Bulk Carrier with an Energy Saving Device'. Proc. Asia Navigation Conference, pp 37-38.

Sahab, A., Meyer, P., Abdel-Maksoud, M. (2022), 'Experimental investigation on the wake of the Japan bulk carrier model with stereoscopic and tomographic particle image velocimetry', 34th Symposium on Naval Hydrodynamics, Washington, USA.

Shevchuk, I, Sahab, A., Abdel-Maksoud, M. (2020), 'Experimental and numerical studies of the flow around the JBC hull form at straight ahead condition and 8° drift angle', 33rd Symposium on Naval Hydrodynamics

Sumislawski, P., Sahab. A., Shevchuk, I., Abdel-Maksoud, M. (2022), 'Numerical investigation of the JBC hull and propeller interaction under static drift condition', 34th Symposium on Naval Hydrodynamics, Washington, USA.